VERSION JANUARY 9, 2014: FM
Preprint typeset using LaTeX style emulateapj v. 11/10/09

SLAC-PUB-15871

UNVEILING THE NATURE OF THE UNIDENTIFIED GAMMA-RAYS SOURCES VIII: COMPUTING THE ASSOCIATION PROBABILITY

F. MASSARO[1], R. D'ABRUSCO[2], N. MASETTI[3], N. OMODEI[1], HOWARD A. SMITH[2] & S. FUNK[1]

version January 9, 2014: fm

ABSTRACT

Despite the significant improvements of the *Fermi* satellite on the source localization with respect to the previous γ-ray missions, the positional uncertainties of the *Fermi* sources are still large, making the search for potential low-energy counterparts a challenging task. In the *Fermi* source catalogs (i.e., 1FGL and 2FGL, respectively) for each counterpart associated with an high-energy source a corresponding value of the association probability was provided. Thus several methods based on the source position or on the logN-logS distribution of potential counterparts were developed to derive the association probabilities. Recently, we discovered a tight connection between the infrared (IR) surveys and the γ-ray sky that allowed us to create several lists of γ-ray blazar-like sources, potential counterparts of *Fermi* objects. Here we complete our previous analyses presenting a new approach based on Montecarlo simulations to determine the association probability for γ-ray blazar-like sources selected on the basis of their peculiar IR colors. We also describe a different version of the likelihood ratio technique with some improvements based on the IR-γ-ray connection. Both methods are compared with the 2FGL associations to asses their reliability. We found reliable counterparts for 39 previously unidentified γ-ray sources listed in the 2FGL and 5 new γ-ray blazar candidates out of 20 sources associated for a subsample of the 1FGL not detected in the 2FGL. Both methods are also able to associate radio loud narrow line Seyfert 1 showing blazar-like IR colors.

Subject headings: methods: statistical - galaxies: active - quasars: general - surveys - radiation mechanisms: non-thermal

1. INTRODUCTION

The association of γ-ray sources with their low-energy counterparts detected in different radio, infrared (IR), optical or X-ray surveys is essential to understand their origin. Despite the recent improvements achieved by the *Fermi* satellite in the source localization (Atwood et al. 2009), the association of *Fermi* objects with their proper counterparts is still unsolved since about one third of sources listed in the second *Fermi*-Large Area Telescope (LAT) catalog (2FGL Nolan et al. 2012) are unassociated.

In Figure 1 we show the comparison between the distribution of the positional uncertainties reported in the 2FGL with those of the 70 months catalog (Baumgartner et al. 2013) of the Burst Alert Telescope (BAT) (Barthelmy et al. 2005) on board of the SWIFT satellite (Gehrels et al. 2004) scanning the sky in the hard X-ray band. It is clear how the *Fermi* positional uncertainty is still a factor of $\sim$5 larger than that in the hard X-rays, being also larger than those at lower energies.

Given the large positional uncertainties in the γ-ray catalogs, a basic requirement for their preparation is providing the association probability computed for each listed counterpart. Thus, several methods have been developed to accomplish the association task, in particular for the γ-ray sources (Mattox et al. 1997; Abdo et al. 2010a). There are basically two main procedures widely accepted to determine the counterparts while comparing different surveys and/or catalogs (e.g. Sutherland & Saunders 1992). The first is matching the nearest neighbor of the unidentified object above the flux limit of the comparison catalog, while the second is using the likelihood ratio technique. In particular, the latter procedure, originally proposed by Ritcher (1975) and subsequently applied by and modified by de Ruiter, Willis & Arp (1977), Prestage & Peacock (1983), Wolstencroft et al. (1986) or more recently by Sutherland & Saunders (1992) and Masci et al. (2001) was successfully used to prepare both the first and the second LAT AGN catalogs (1LAC and 2LAC Abdo et al. 2010b; Ackermann et al. 2011, respectively).

Recently, we discovered a tight connection between the IR colors and the γ-ray spectral shape occurring for the largest known population of *Fermi* sources: the blazars (Massaro et al. 2011a; D'Abrusco et al. 2012). They are the rarest among the AGN classes which emission is interpreted as due to ultrarelativistc particles accelerated in a jet closely aligned to the line of sight (Blandford & Rees 1978; Urry & Padovani 1995). Blazars come in two main flavors: the low luminosity class, constituted by BL Lac objects, characterized by featureless optical spectra, and the flat-spectrum radio quasars with optical spectra typical of quasars (Stickel et al. 1991; Stoke et al. 1991; Laurent-Muehleisen et al. 1999). In the following the former class is labeled as BZBs while the latter one as BZQs, according to the nomenclature proposed in the Multiwavelength Blazar Catalog[4] (Roma-BZCAT,

[1] SLAC National Laboratory and Kavli Institute for Particle Astrophysics and Cosmology, 2575 Sand Hill Road, Menlo Park, CA 94025, USA
[2] Harvard - Smithsonian Astrophysical Observatory, 60 Garden Street, Cambridge, MA 02138, USA
[3] INAF Istituto di Radioastronomia, via Gobetti 101, 40129, Bologna, Italy

[4] http://www.asdc.asi.it/bzcat/

KIPAC, SLAC National Accelerator Laboratory, 2575 Sand Hill Road, Menlo Park, CA 94025
Work supported in part by US Department of Energy under contract DE-AC02-76SF00515.

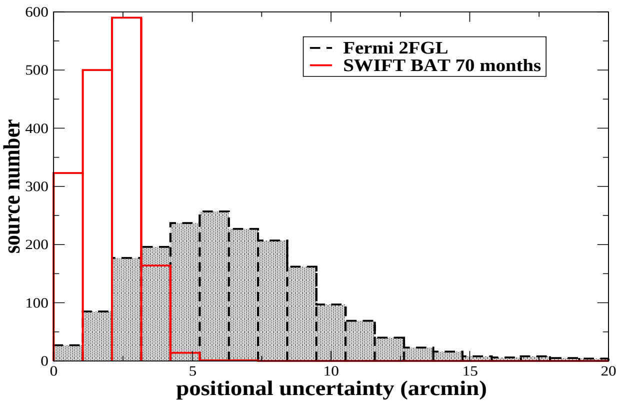

Fig. 1.— The distributions of the positional uncertainty radius at 95% level of confidence for the *Fermi* sources that belong to the 2FGL (black) (Nolan et al. 2012) in comparison with those in the 70 months catalog of SWIFT - BAT (red) (Baumgartner et al. 2013). For the *Fermi* positional uncertainties, being elliptical regions, we computed the radius shown above as the square root of the product between the semi major and the semi minor axes of the ellipse.

Massaro et al. 2009; Massaro et al. 2011b).

Using the IR colors derived from Wide-field Infrared Survey Explorer (*WISE*) all-sky survey [5] (Wright et al. 2010) alone (Massaro et al. 2012b; D'Abrusco et al. 2013) or in combination with other multifrequency observations (Paggi et al. 2013; Massaro et al. 2013b), we developed an association method to determine γ-ray blazar-like sources that could be potential counterparts of the *Fermi* UGSs (see also Massaro et al. 2013c; Massaro et al. 2013a). We are carrying on follow up campaigns, mostly via optical spectroscopy, to determine the nature of these potential counterparts and to validate our associations (e.g., **?** Cowperthwaite et al. 2013). Moreover on the basis of this IR-γ-ray connection we also extracted a catalog of γ-ray blazar-like source selected on the basis of their IR colors and having a radio counterpart: namely the *WISE* blazar candidate (WBC) catalog (D'Abrusco et al. 2014).

The number of UGSs mostly decreased thanks to our IR based association procedure and confirmed by the preliminary results of our optical campaigns or those of other colleagues (see also Masetti et al. 2013a; Paggi et al. 2014). However we still have to compute the association probability for each γ-ray blazar-like source to complete our analysis and to asses the reliability of our associations as in the *Fermi* catalogs. In this last paper of the series, we propose two procedures to compute this association probability. The first method is based on the sky distribution of the WBC catalog and uses Montecarlo simulations, while the second one is a variation of the likelihood ratio technique based on the IR color distribution of the γ-ray blazar-like sources.

The paper is organized as follows: in Section 2 we described the *WISE* and the *Fermi* catalogs adopted for our analysis, and in Section 3 we described our procedures to determine the association probabilities. Results are given in Section 4 while a comparison with previous γ-ray analyses in Section 5. Finally, Section 6 is devoted to our summary and conclusions. For our numerical results, we use cgs units unless stated otherwise. Spectral indices, α, are defined by flux density, $S_\nu \propto \nu^{-\alpha}$ and *WISE* magnitudes at the [3.4], [4.6], [12], [22] μm (i.e., the nominal *WISE* bands) are in the Vega system respectively; we also label the IR colors as $c_{12} = [3.4] - [4.6]$ and $c_{34} = [12] - [22]$.

[5] In this paper the new version of the *WISE* catalog (i.e., ALLWISE data release) have been used. See http://wise2.ipac.caltech.edu/docs/release/allwise/ for details.

2. CATALOGS USED IN OUR INVESTIGATION

To achieve our goal we used the recent catalog of γ-ray blazar-like sources (i.e., hereinafter the WBC catalog) extracted from the ALLWISE sky survey (Wright et al. 2010) as described in D'Abrusco et al. (2014). It lists 11429 γ-ray blazar blazar-like sources selected having the same IR colors of the known population of *Fermi* blazars and with a radio counterpart in one of the three major radio surveys: the NRAO VLA Sky Survey Catalog (NVSS; Condon et al. 1998), the Faint Images of the Radio Sky at Twenty centimeter] (FIRST; Becker et al. 1995; White et al. 1997) and the Sydney University Molonglo Sky Survey (SUMSS; Mauch et al. 2003).

We compared the WBC catalog with the 2FGL that is the most recent *Fermi* catalog available. Then, we also run our procedures on the subsample of the 1FGL catalog that includes *Fermi* sources not listed in the 2FGL (Abdo et al. 2010a).

Although the 2FGL catalogs lists 1873 *Fermi* sources only 1860 have a reported positional uncertainty that is a minimal requirement to search for a potential counterpart, the same situation occurs for the 1FGL where there are 1393 γ-ray sources with a non-null value of the positional uncertainty out of 1451 listed in the whole catalog. Those γ-ray sources lacking of the positional uncertainties are identified pulsars for which the radio positions are reported in both the 1FGL and the 2FGL catalogs rather than their γ-ray ones.

Hereinafter when we refer to the 2FGL catalog we considered the subsample selected on the basis of their positional uncertainty. We noted that 1099 sources out of the 1393 present in the 1FGL also belong to the 2FGL, then the remaining 294 constitute the 1FGL subsample analyzed in the following. All the details about the γ-ray analysis and the discrepancies between the *Fermi* two catalogs have been extensively discussed in Nolan et al. (2012). We only analyzed separately both 1FGL and 2FGL samples to verify the presence of γ-ray blazar-like sources associable with 1FGL sources that are not listed in the 2FGL.

Finally, we highlight that in the following analysis we did not exclude the *Fermi* sources that are listed in the 1FGL subsample or in the 2FGL with a gamma-ray analysis flag as done in our previous investigations (e.g., Massaro et al. 2012b; Massaro et al. 2013c).

3. METHODS TO ESTIMATE THE ASSOCIATION PROBABILITIES

3.1. *Positional method based on Montecarlo simulations*

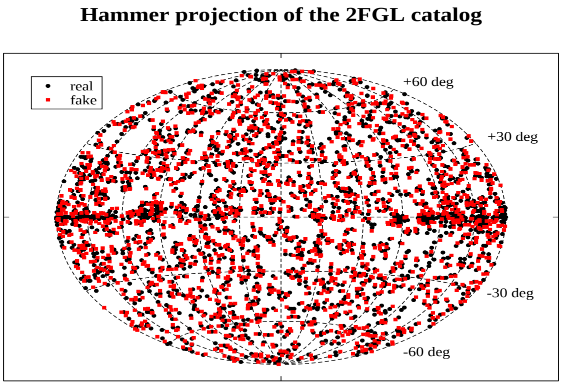

FIG. 2.— The comparison between the sky distribution of the *Fermi* sources in the 2FGL and those in one of the η fake catalogs generated by shifting their γ-ray positions of the objects in a random direction. It is clear how the sky distribution of the sources is preserved in the fake catalog. The shift used to create the fake catalogs has a fixed length of 2° (see Section 3.1 for more details).

This first method assigns a value of the association probability to all the γ-ray blazar-like source that lie within the positional uncertainty region of a *Fermi* source. Once this probability is assigned a γ-ray blazar-like source could be considered a candidate counterpart of the corresponding *Fermi* object.

We computed the probability that a real crossmatch occurring at angular separation R_{real} can be spurious comparing η fake replicas of the 2FGL with the WBC catalog. This procedure takes into account the sky distribution of both the *Fermi* and the WBC sources. Here we described this method step-by-step.

1. We crossmatched the WBC catalog with all the position of the N sources in the 2FGL to compute the distribution of the real angular separations between the two catalogs. The initial, arbitrary, radius adopted to perform the crossmatch was chosen larger than the maximum semi major axis among all the positional uncertainties ellipses at 99.9% level of confidence.

2. We created a number η of fake γ-ray catalogs by shifting the positions of each γ-ray source in the 2FGL in a random direction of the sky by a fixed length L_{rand}.

The shift L_{rand} to create the fake γ-ray catalogs has to be larger than the largest positional uncertainty region reported in the 2FGL ($\sim$1°) but not too distant from the original location of the *Fermi* source. This guarantees to obtain fake catalogs with a sky distribution similar to the original 2FGL and to have crossmatches between each fake and the WBC catalog that takes into account the local density distribution of the candidate counterparts. Creating the fake γ-ray catalogs, we adopted the constraint that no real γ-ray sources has to be located within the positional uncertainty region at 99.9% level of confidence of each fake object. We tried different values for L_{rand} between 1°and 5° and then we chose $L_{rand} = 2°$ (similar to the value adopted by Ackermann et al. 2011). The total number of γ-ray sources in each fake 2FGL replica is also preserved being equal to that in the real one. An example of the sky distribution of one of the fake 2FGL catalogs is shown in Figure 2 in comparison with the real one.

3. We considered an angular separation R, and we counted the number of *Fermi* sources $n(R)$ having at least one WBC correspondence occurring at angular separation $R_{real} < R$. Our first choice of R as set to 10″.

4. For each fake replica of the 2FGL, we counted the number of fake γ-ray sources $n_{fake,i}(R)$ having at least one WBC counterpart at angular separation R_{fake} smaller than R.

5. We calculated the mean number $\lambda(R)$ of fake associations occurring at angular separation $R_{fake} < R$, averaged over the η fake catalogs as $\lambda(R) = \sum_i^{\eta} n_{fake,i}(R)/\eta$. and its variance σ^2.

The distribution of n_{fake} at each angular separation is Poissonian being also clear since $\lambda = \sigma^2$. To verify accurately this condition we found that the minimum number of fake 2FGL η built has to be larger than $\sim$50. The value adopted in our simulations is η =100. We then proceeded as follows to determine the probability of spurious associations as function of the angular separation.

6. We increased the radius by ΔR and we computed the difference $\Delta n(R)$ and $\Delta \lambda(R)$ defined as:

$$\Delta n(R) = n(R + \Delta R) - n(R) \quad (1)$$

$$\Delta \lambda(R) = \lambda(R + \Delta R) - \lambda(R)\,, \quad (2)$$

The ΔR value adopted in our calculation is 10″. This value has been chosen to be at least one of order of magnitude smaller than the *Fermi* typical positional uncertainty. However we remark that it is also possible to increase the radius multiplying the previous one by a factor of $\sqrt{2}$, so to have annuli of equal area and the results are unchanged.

7. When we found the first radius R_1 at which $\Delta \lambda$ is equal to 1 within 1σ, we stopped and we computed the ratio:

$$f(R_1) = \frac{1}{N - n(R_1)} \quad (3)$$

where the difference $N - n(R_1)$ is the number of remaining *Fermi* source to be associated at radius larger than R_1.

The ratio $f(R_1)$ is the probability to find one spurious association within the angular separation R, since the numerator of Eq. 3 is the number of favorable events while $N - n(R_1)$ is the number of possible events.

8. We iterate the above procedure by increasing the radius of ΔR and recounting $n(R_k)$ as Δn and $\Delta \lambda$, obtained in each annulus $\Delta(R)$. We stopped at each radius R_k every time we reached the condition $\Delta \lambda$ =1 within 1σ range computing the ratio

$$f(R_k) = \frac{1}{N - n(R_k)}\,. \quad (4)$$

The $f(R_k)$ curve obtained is shown in Figure 3.

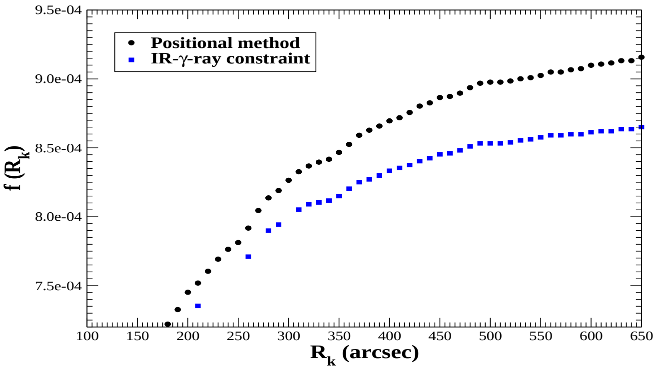

FIG. 3.— The curves for the ratio $f(R_k)$ computed using the Positional method when comparing the 2FGL and the WBC. The black circles refers to the simple procedure while the blue squares to the implemented procedure taking into account the IR-γ-ray correlation (see Section 3.1 for details).

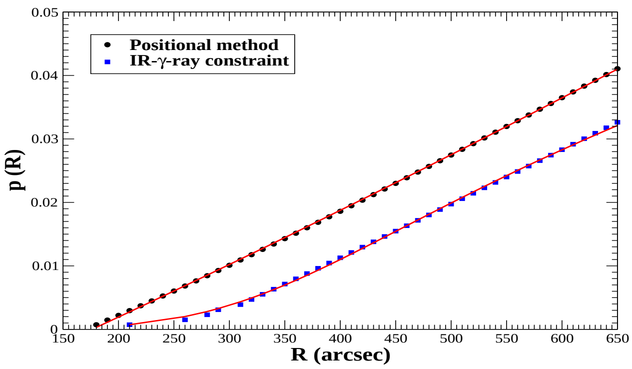

FIG. 4.— The probability curve $p(R)$ computed using the Positional method when comparing the 2FGL and the WBC. The black circles refers to the simple procedure while the blue squares to the implemented procedure taking into account the IR-γ-ray correlation (see Section 3.1 for details). The best fit regression curves are indicated by the solid red lines.

9. Adding all the values obtained for $f(R_k)$ we can compute the probability that a generic source lying at angular separation smaller than R_Q is a spurious association according to the following equation:

$$p(R_Q) = \sum_{k=1}^{Q} f(R_k) \ . \qquad (5)$$

Finally, interpolating $p(R_Q)$ we obtained the probability curve $p(R)$. For the comparison between the 2FGL and the WBC, $p(R)$ is plotted in Figure 4. This allows us to compute $p(R_{real})$ for each WBC source lying at angular separation R_{real} from the closest 2FGL object.

10. We also derived a reliability threshold by comparing the $\Delta\, n(R)$ and $\Delta\, \lambda(R)$. We considered reliable only sources at angular separation $R_{real} < R_{th}$ =500″, where this radial threshold R_{th} is set to the first R value for which $\Delta\, \lambda(R) > \Delta\, n(R)$.

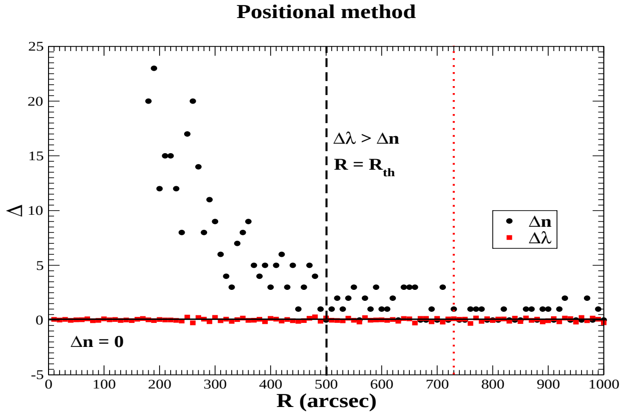

FIG. 5.— The values of $\Delta\, \lambda(R)$ (red squares) and $\Delta\, n(R)$ (black circles) as function of the angular separation R for the positional method based on the Montecarlo simulations. We restricted the y axis to $\Delta\, \lambda(R)$ and $\Delta\, n(R)$ values below 25. Our conservative choice of R_{th} is marked by the vertical dashed line. It occurs at the first R value for which $\Delta\, \lambda(R) > \Delta\, n(R)$. The dotted, vertical, red line indicates a different threshold that could be choose.

This implies that when considering associations occurring at R_{th} there is higher chance to obtain a fake crossmatch than a real one.

To simplify the calculation of $p(R_{real})$, we approximated the $p(R)$ curves with the following function:

$$p(R) = C \cdot \frac{R^{a+1}}{R^a + R_o} \qquad (6)$$

in the range of angular separations $[0, R_{th}]$.

It is worth noting that different choices of R_{th} can be assumed as for example considering the first radius at which the fluctuations of $\Delta\, \lambda(R)$ are similar to those of $\Delta\, n(R)$, that for the comparison between the 2FGL and the WBC catalogs occurs at 730″(see Figure 5). In addition, we note that the $\Delta\, \lambda(R)$ and the $\Delta\, n(R)$ curves could be fitted to simplify the search for R_{th}.

11. Since $n_{fake}(R)$ follows the Poisson distribution with the expected value λ, we can also compute the probability of having a total number of $n(R)$ associations according to the formula:

$$P_{all}(R) = e^{-\lambda}\, \frac{\lambda^n}{n!} \ . \qquad (7)$$

This is the probability of finding all the crossmatches occurring within angular separation R by chance. It is worth noting that the total $n \gg \lambda$ thus it is possible to approximate the probability derived from Equation 7 using the Stirling formula and computing its logarithm as:

$$log\, P_{all}(R) = (n-\lambda) loge - \frac{1}{2} log(2\pi\, n) + nlog\left(\frac{\lambda}{n}\right) \ . \quad (8)$$

In Figure 6 we show the values computed for $log\, P_{all}$ as function of the angular separation R. The extremely low values of $log\, P_{all}$ indicates that the two catalogs matches very well together strengthening the reliability of our candidates. This curve could be also used to select the radial threshold R_{th}, for example at the minimum values

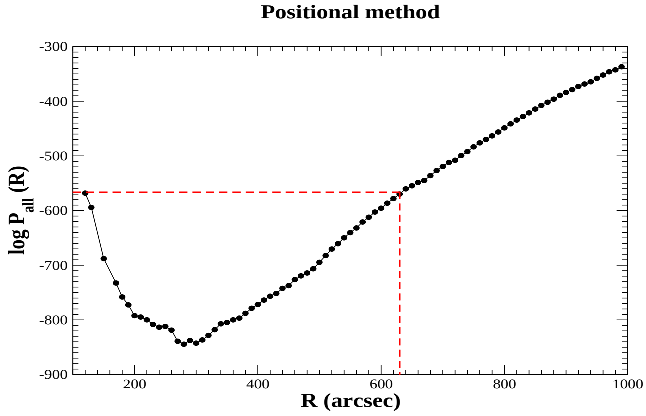

FIG. 6.— The probability P_{all} that all the crossmatches occurring at angular separation R could be spurious associations. The red dashed lines mark the value of the angular separation at which $log\, P_{all}$ has the same value achieved at the first association radius.

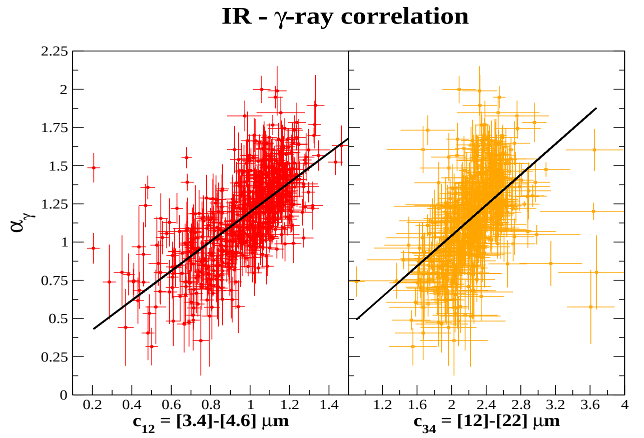

FIG. 7.— The correlations between the γ-ray spectral index α_γ and the IR colors c_{12} (left panel) and c_{34} (right panel) known for the *Fermi* blazars (D'Abrusco et al. 2012).

of $log\, P_{all}$ or when it reaches the same value that occurs at the first association radius.

The method described above can be also implemented taking into account the known correlation between the IR and the γ-ray spectral shapes occurring to the *Fermi* blazars. The constraint set on the angular separation to compute $\Delta\, n(R)$ and $\Delta\, \lambda(R)$ can be strengthen considering the one derived from the IR-γ-ray spectral index correlation known for *Fermi* blazars (e.g., Figure 7 and see also D'Abrusco et al. 2012; Massaro et al. 2012b).

As shown in Figure 7 the IR colors correlate with the γ-ray spectral index. Thus when counting $n(R)$ and the $\lambda(R)$ for a given real or fake γ-ray source of spectral index α_γ, we added the constraint that the WBC sources must have the IR colors consistent with the IR-γ-ray correlations within 3σ range. Also in this case the radial threshold R_{th}, computed according to the previous criterion, corresponds to $500''$ (see Figure 8).

There are advantages on using the additional constraint on the IR-γ-ray correlations. The probabilities to have spurious associations derived adopting this constraint are smaller than those derived when taking into account only of the angular separation as shown in Figure 4. The first radius at which the condition $\Delta\, \lambda = 1$ occurs at larger distances than for the simple positional method making the associations more reliable and physically justified.

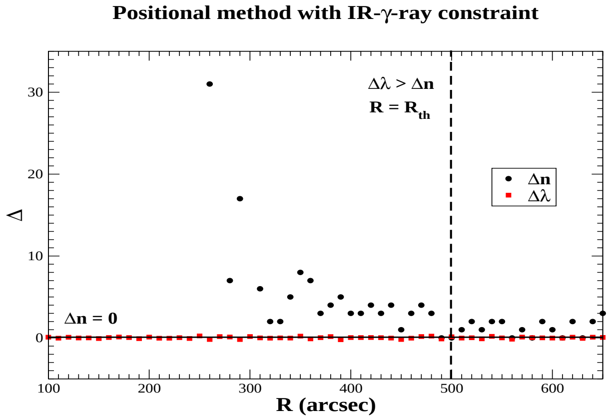

FIG. 8.— Same of Figure 8 computed with the positional method but taking into account the constraint on the IR colors. We restricted the y axis to $\Delta\, \lambda(R)$ and $\Delta\, n(R)$ values below 35.

Finally, we emphasize that it is possible to take into account the *Fermi* point spread function (PSF) a posteriori to determine the most reliable associations. Once the radial threshold is selected and all the associations are computed, we performed the crossmatches taking into account the elliptical shape of the positional uncertainty regions reported in both the *Fermi* (Nolan et al. 2012) and WBC catalog (Cutri et al. 2012). Then we selected only the sources having angular separation $R_{real} < R_{th}$ and within the positional uncertainty regions at a 95% level of confidence to compare our results with the 2LAC and 2FGL catalogs.

3.2. *The likelihood ratio procedure*

Our second procedure adopted to estimate the association probability is a variation of the likelihood ratio method described in Sutherland & Saunders (1992) and adopted by Ackermann et al. (2011) for the 2LAC.

1. We crossmatched the WBC catalog with the 2FGL to create the list of all the γ-ray blazar-like sources that lie within the positional uncertainty region at 95% level of confidence of each *Fermi* object. The results of this crossmatch corresponds to all the potential counterpart of the 2FGL sources: N_{real}.

For the 2FGL sources, the elliptical uncertainty regions have the semi major axis (i.e., θ_{68}) and the semi minor axis (i.e., ϑ_{68}) at 68% level of confidence reported in the 2FGL (e.g., Nolan et al. 2012).

As previously described in Section 3.1, we also took into account the IR-γ-ray correlation to select the sources in the WBC catalog when computing this crossmatch. However, for the likelihood ratio method, we explored a different procedure, that we verified a posteriori being in agreement with the previous one. This allowed us to take into account the uncertainty on the γ-ray spectral index. This reduces the surface density of WBC sources by $\sim$10-15% depending on the value of α_γ.

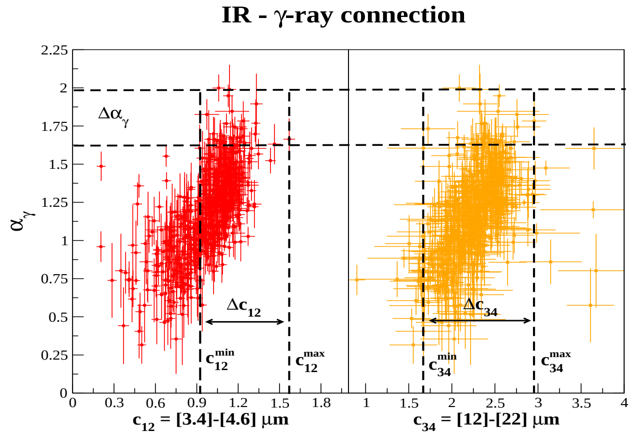

FIG. 9.— The relations between the γ-ray spectral index α_γ and the IR colors c_{12} (left panel) and c_{34} (right panel) for the known *Fermi* blazars. The range $\Delta\alpha_\gamma$ and the corresponding $\Delta\, c_{12} = [c_{12}^{min}, c_{12}^{max}]$ and $\Delta\, c_{34} = [c_{34}^{min}, c_{34}^{max}]$ intervals are also indicated by the dashed black lines in each panel, for a generic source having $\alpha_\gamma = 1.75$ and $\sigma_\gamma \simeq$0.1.

For each 2FGL source, we considered the interval $\Delta\alpha_\gamma = [\alpha_\gamma \pm 1\sigma_\gamma]$. Then, given the relations between α_γ and c_{12} and c_{34}, respectively, we selected from the WBC catalog only those sources with IR colors within the ranges $\Delta\, c_{12} = [c_{12}^{min}, c_{12}^{max}]$ and $\Delta\, c_{34} = [c_{34}^{min}, c_{34}^{max}]$ corresponding to the $\Delta\alpha_\gamma$ interval, as shown in Figure 9. This subset of the WBC catalog has been used to perform the crossmatch between the real catalogs.

2. For all the potential counterparts of each γ-ray source we calculated the dimensionless difference between the *WISE* (i.e., α_i, δ_i) and the *Fermi* (i.e., α_k, δ_k) positions according to the equation:

$$r_{ik} = \left[\frac{(\alpha_i - \alpha_k)^2}{\sigma_{\alpha_i}^2 + \sigma_{\alpha_k}^2} + \frac{(\delta_i - \delta_k)^2}{\sigma_{\delta_i}^2 + \sigma_{\delta_k}^2} \right]^{1/2} , \qquad (9)$$

where $\sigma_{\alpha_{i,k}}$ and $\sigma_{\delta_{i.k}}$ are the uncertainties on the right ascensions ($\alpha_{i,k}$) and the declinations ($\delta_{i,k}$) for both the *WISE* and the *Fermi* position, respectively (see Masci et al. 2001, for the r_{ik} formula).

While the *WISE* catalog (Wright et al. 2010; Cutri et al. 2012) reports the uncertainties on the right ascensions and on the declinations (i.e., σ_{α_i} and σ_{δ_i}, respectively), these are not listed in the *Fermi* catalogs that instead provides the semi major axis (i.e., θ_{68}), the semi minor axis (i.e., ϑ_{68}) and the position angle (i.e., PA) of the elliptical uncertainty region at 68% level of confidence. Thus we computed the uncertainties on the *Fermi* right ascensions and declinations according to the following relations:

$$\sigma_{\alpha_k}^2 = \theta_{68}^2\, sin^2(PA) + \vartheta_{68}^2\, cos^2(PA) \qquad (10)$$

$$\sigma_{\delta_k}^2 = \theta_{68}^2\, cos^2(PA) + \vartheta_{68}^2\, sin^2(PA) \qquad (11)$$

as, for example, shown in Cutri et al. (2012)[6].

[6] http://vizier.u-strasbg.fr/viz-bin/VizieR-n?-source=METAnot&catid=2311&notid=6&-out=text

3. For each IR counterpart we computed the likelihood ratio LR_{ik} derived from the following equation:

$$logLR_{ik} = log \left[\frac{Q(\Delta\, c_{12}, \Delta\, c_{34})}{N(\Delta\, c_{12}, \Delta\, c_{34})} \cdot f(r_{ik}) \right] , \qquad (12)$$

where $Q(\Delta\, c_{12}, \Delta\, c_{34})$ is the probability to find a WBC source with the IR colors within the ranges $\Delta\, c_{12}$ and $\Delta\, c_{34}$ over the entire catalog, while $N(\Delta\, c_{12}, \Delta\, c_{34})$ is the local surface density of WBC sources having IR colors within the same ranges. The function $f(r_{ik})$ is the distribution function of the normalized angular separations (i.e., the Gaussian distribution, the same adopted in the previous analyses, e.g., Sutherland & Saunders 1992; Ackermann et al. 2011):

$$f(r_{ik}) = \frac{e^{-r_{ik}^2}}{2\pi \cdot \sqrt{(\sigma_{\alpha_i}^2 + \sigma_{\alpha_k}^2)\,(\sigma_{\delta_i}^2 + \sigma_{\delta_k}^2)}} . \qquad (13)$$

The quantity $Q(\Delta\, c_{12}, \Delta\, c_{34})$ has been computed as the ratio between the number of WBC sources having IR colors in the ranges $\Delta\, c_{12}$ and $\Delta\, c_{34}$ and the total number of WBC sources. On the other hand, $N(\Delta\, c_{12}, \Delta\, c_{34})$ is the surface density of the "background" objects at the appropriate Galactic latitude within a circular region centered on the 2FGL source position with 6° radius. It is worth noting that $N(\Delta\, c_{12}, \Delta\, c_{34})$ was not be evaluated using the IR color distributions of the entire WBC catalog but it was restricted to the same range of colors of $Q(\Delta\, c_{12}, \Delta\, c_{34})$.

The underlying reason of considering the local surface density of "background" IR sources resides in the possibility that within the WBC catalog there could be a contaminant population of Galactic origin with a surface density dependent by sky position. So computing $N(\Delta\, c_{12}, \Delta\, c_{34})$ locally reduces the effect of a source density increased because of the presence of Galactic sources at least above and below the Galactic plane. We also remark that computing $N(\Delta\, c_{12}, \Delta\, c_{34})$ locally permits to mitigate possible effects of non-uniform *WISE* sky coverage (significant at scales larger than $\sim$10°) corresponding to a non-uniform flux limit in the WBC catalog used for the comparison.

At this step we have a value of $log\, LR_{ik}$ for each WBC source correspondent to a *Fermi* object in the 2FGL. Then we proceed computing the $log\, LR_{ik}$ threshold at which we can consider our candidates reliable. Such reliability threshold is calculated generating η fake replicas of the 2FGL catalog, crossmatching them with the real WBC catalog and determining the LR_{ik} distributions for the fake potential associations (see steps 4 to 6 below).

4. Similarly to the previous method, we created a number η of fake γ-ray catalogs by shifting the positions of each γ-ray source in the 2FGL in a random direction of the sky and ensuring that there are no real *Fermi* sources located within the positional uncertainty region at 99.9% level of confidence for all the fake objects. The procedure to estimate the reliability threshold via Montecarlo simulations has been also used by Lonsdale et al. (1998).

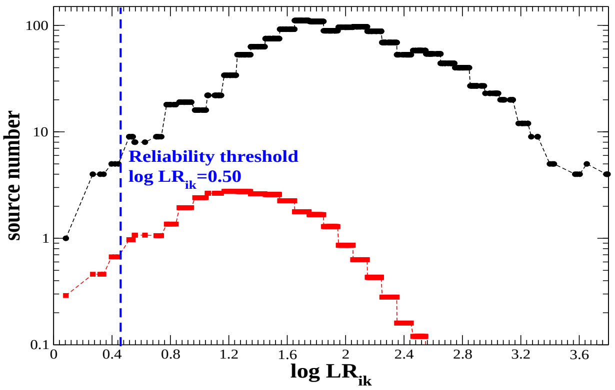

FIG. 10.— Left panel) The distribution of both N_{real} (black circles) and $< N_{fake} >$ (red square) as function of the $log\, LR_{ik}$. The reliability threshold chosen in our analysis is indicated by the vertical, blue dashed line.

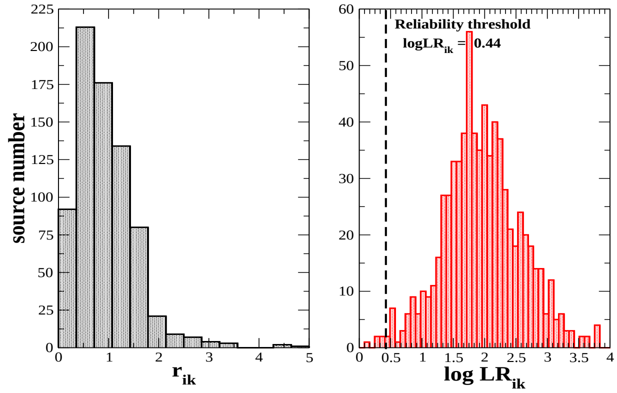

FIG. 11.— Left panel) The distribution of the dimensionless angular separation r_{ik} computed between the real sources in the 2FGL and their potential counterparts in the WBC catalog. Right panel) The distributions of the $log\, LR_{ik}$ for the real associations. The reliability threshold chosen in our analysis is indicated by the vertical dashed line. The distribution of r_{ik} is shown between the values of 0 and 5 while that of $log\, LR_{ik}$ between 0 and 4.

5. We repeated the calculation of $log\, LR_{ik}$ for all the sources that belong to the η fake catalogs to compute the total distribution function of fake LR_{ik} and the average value of $< N_{fake}(LR_{ik}) >$.

$$< N_{fake}(LR_{ik}) >= \frac{1}{\eta} \sum_{j}^{\eta} N_{fake,j} \; . \qquad (14)$$

We note that the total number of fake catalogs generated for our investigation is determinate by the condition: $\sum_j^{\eta} N_{fake,j} \geq N_{real}$.

6. We compared the real and the fake distributions of $log\, LR_{ik}$ to determine the reliability threshold for the real associations computing:

$$\rho(LR_{ik}) = 1 - \frac{< N_{fake}(LR_{ik}) >}{N_{real}(LR_{ik})} \; . \qquad (15)$$

The reliability computed according to Equation 15 represents an approximate measure of the association probability for a potential counterpart having a given $log\, LR_{ik}$ (e.g., Masci et al. 2001).

As shown in Figure 10 the difference between N_{real} and $< N_{fake} >$ is almost constant at low values on $log\, LR_{ik}$ where the two curves rise similarly as function of $log\, LR_{ik}$. Thus, we chose as reliability threshold for our associations the latest values of $log\, LR_{ik}$ for which the difference between N_{real} and $< N_{fake} >$ is almost constant, corresponding to $log\, LR_{ik}$ =0.44.

In Figure 11, we also show the distribution of the dimensionless angular separation r_{ik} computed for the WBC sources that lie within the positional uncertainty regions at 95% level of confidence of each 2FGL source together with their $log\, LR_{ik}$ distributions between 0 and 4.

4. RESULTS

Once the reliability thresholds were chosen, we computed and compared the results of both our association methods with those of the 2FGL and with the 1FGL subsample (see Section 2 for more details). To prepare the final list of our associations we considered only the counterparts of the WBC lying within the *Fermi* positional uncertainty regions at 95% level of confidence so to compare the positional method with the modified likelihood ratio procedure.

The total number of potential candidates in the WBC catalog for the 2FGL sources is 750 with 5 double matches. The first method has 724 potential counterparts (including 3 out of 5 double matches) below the reliability threshold $R_{th} = 500''$. In detail, according to the 2FGL classification: 4 sources are generic active galactic nuclei (AGNs), 115 are AGN of uncertain type (AGUs) with 1 double matches, 311 BZBs (1 double matches), 252 BZQs (1 double matches), 3 Seyfert galaxies (SEYs), 2 radio galaxies (RDGs), 37 UGSs. While considering the IR-γ-ray constraint, the method provides 682 associations with respect to the previous one. Their list includes: 4 AGNs, 97 AGUs, 297 BZBs (1 double matches), 238 BZQs (1 double matches), 2 SEYs, 2 RDGs, 31 UGSs. All the associations found using the positional method with the constraint on the IR colors were found by the positional procedure, but with higher probabilities. This is due to the same radial threshold R_{th} chosen for the two procedures.

On the other hand, the likelihood modified procedure provides 725 associations (including 7 double matches) above the $log\, LR_{ik}$ threshold of 0.44, listing: 3 AGNs, 109 AGUs, 300 BZBs with 1 double match, 242 BZQs with 2 double matches, 3 SEYs, 2 RDG, 1 candidate extended source (SPP) and 39 UGSs with 1 double match. It is worth noting that all the associations computed with the LR method were also found with the positional procedure, with the only exception of 17 objects, 15 already known in the 2LAC and 2 UGSs. A similar situation occurs when comparing the LR method with the positional method implemented by the IR-γ-ray constraint, where the discrepancy in their results is limited to 15 sources, 14 known and 1 UGS.

There are 23 sources out of the 750 2FGL associations (1 AGN, 7 BZBs, 13 BZQs and 1 SEY) that due to their variability simultaneously detected at lower energies than the *Fermi* range are indicated in the 2FGL as "identified" rather than "associated" and all of them were found with all our methods.

We also applied our calculation of the association probabilities also to the subsample of the 1FGL catalog previously defined (see Section 2 for more details) adopting the same reliability thresholds. Also in this case the results are in agreement with the associations of the 1FGL and the 1LAC. We found a total of 20 crossmatches between the WBC catalog and the 1FGL with only 2 double matches. In detail, according to the 1FGL classifications the positional method finds 1 AGNs, 2 AGUs, 5 BZBs with 1 double match, 5 BZQs, 5 UGSs. While considering the IR-γ-ray constraint on the IR colors, there are 1 AGNs, 2 AGUs, 3 BZBs 4 BZQs, 5 UGSs, all included in the previous list and with no double matches. Then, the likelihood modified procedure provides: 1 AGN, 2 AGUs, 5 BZBs with 1 double match, 7 BZQs and 5 UGSs.

In Table 1 we listed all the 750 2FGL candidate counterparts with their values of the probabilities derived with all procedures. For all these WBC sources we report the 2FGL name, the name of the *WISE* counterpart and its coordinates with the probabilities derived from both the positional method with and without the constraint on the IR colors and together with the $log\, LR_{ik}$ values. We also report the class assigned by the 2FGL/2LAC associations and the name of the 2LAC counterpart. On the other hand, Table 2 summarizes all these 1FGL associations with their values of the probabilities as for Table 1. Finally, we remark that none of PSRs listed in the second pulsar LAT catalog (Abdo et al. 2013) has a WBC source located within their *Fermi* positional uncertainty regions at 95% level of confidence.

5. COMPARISON WITH PREVIOUS ANALYSES

5.1. *First method: the Montecarlo based technique*

We compare the positional method based on the Montecarlo simulations with the Bayesian procedure proposed by Mattox et al. (1997) to associate flat spectrum radio sources then refined and used in both the 1FGL (Abdo et al. 2010a) and the 2FGL (Nolan et al. 2012).

Both methods compute the probability to find a spurious associations within a given angular separation from the position of a γ-ray source. However there are several differences between these two procedures.

The Bayesian method assumes an a priori probability density function for a counterpart to lie at angular separation R from the location of a γ-ray source. This is in general described as a Gaussian distribution with variance equal to positional uncertainty region at a certain level of confidence. The Bayesian method also assumes an *a priori* probability density function to have a generic source lying at the same angular separation by chance. This is generally computed assuming a constant local density of the background sources in a region close to the location of the γ-ray object. Thus the latter probability density function scales as proportional to the angular separation square (i.e., $\propto R^2$).

The main difference between the two procedures is that for the Bayesian method both the above assumptions are arbitrary while the positional method does not require any a priori hypothesis making our procedure more empirical. It is important to note that the Bayesian method needs to assume a model for the *Fermi* PSF a priori generally used to determine the probability density function for the real associations. Our positional associations are independent by this hypothesis, thus also avoiding any uncertainty due to calibration or incorrect estimates of the positional error regions due to possible systematic uncertainties. On the other hand in our positional procedure it is possible to take into account the PSF a posteriori. A deeper analysis to verify the a priori hypotheses underlying the Bayesian method should be performed to justify the probability calculations.

The Montecarlo based technique takes into account the global match property between the two catalogs. The fact that at given angular separation the number of the real crossmatches is much larger than that of the fakes ones implies a low probability of being random and suggests that the comparison catalog includes many real counterparts. This is can be easily verified computing P_{all}. The positional method takes also into account the sky distribution of both the 2FGL and the WBC sources as well as of their local surface density, since the simulations are computed to preserve both of them.

An additional advantage in the positional method is that the reliability threshold chosen on the radius R_{th}, it is not an arbitrary choice but it can be selected on the basis of the $\Delta\, n(R)$ and $\Delta\, \lambda(R)$ curves to account for the distribution of the real angular separations. This threshold cannot be set to the same value for each comparison catalog used for the counterpart search, since they could have different source densities and thus different probabilities to obtain spurious associations. On the other hand, our positional procedure determines the reliability threshold R_{th} and the probability curve $p(R)$ for each specific comparison catalog used for the counterpart search (i.e., the WBC in the analysis presented here).

We highlight that the implementation of this method based on the IR-γ-ray spectral connection, introduces a physical property that allows us to extend the reliability threshold on the radius beyond the one determined only by the positional condition. It permits to find reliable associations at larger angular separations larger than those com outed with the simple positional method.

Finally, we performed an additional test on the Roma-BZCAT to compare the Bayesian method with our positional procedure. We run the positional procedure on the Roma-BZCAT and we chose as reliability threshold R_{th} =500$''$ to be very conservative as described in Section 3.1. Then we selected in both the 2FGL/2LAC and among our associated sources all the blazars with at angular separation smaller than R_{th} and lying within the positional uncertainty region at 95% level of confidence. We found that our positional procedure provides 23 more associations than the Bayesian procedure, all of them are listed in Table 3. These are all reliable associations because: (i) they all appear in the 2LAC catalog as associated with different methods than the Bayesian one, (ii) they are all confirmed blazars since they belong to the Roma-BZCAT and (iii) they are also confirmed by our positional procedure. Thus we conclude that our procedure could supersede the Bayesian method.

TABLE 1
Association probabilities for 2FGL sources (first 10 lines).

2FGL name	WBC association	R deg.	p pos.	p IR cons.	$log\, LR_{ik}$	ρ	2FGL class	2FGL counterpart
2FGLJ0000.9-0748	J000118.01-074626.9	0.1	0.0146	0.0076	1.33	0.95	bzb	PMN J0001-0746
2FGLJ0004.7-4736	J000435.65-473619.6	0.022	2.0E-4	0.0	1.92	0.99	bzq	PKS 0002-478
2FGLJ0006.1+3821	J000557.18+382015.1	0.032	6.0E-4	0.0	1.74	0.98	bzq	S4 0003+38
2FGLJ0007.8+4713	J000745.09+471130.5	0.045	0.0018	2.0E-4	1.97	0.99	bzb	MG4 J000800+4712
2FGLJ0007.8+4713	J000759.97+471207.7	0.033	6.0E-4	0.0	2.2	1.0	bzb	MG4 J000800+4712
2FGLJ0009.0+0632	J000903.93+062821.2	0.07	0.0063	0.0017	1.75	0.98	bzb	CRATES J0009+0628
2FGLJ0009.1+5030	J000922.75+503028.7	0.034	7.0E-4	0.0	1.95	0.99	agu	NVSS J000922+503028
2FGLJ0011.3+0054	J001130.39+005751.8	0.078	0.0083	0.0029	1.55	0.98	bzq	PMN J0011+0058
2FGLJ0012.9-3954	J001259.89-395425.9	0.0070	0.0	0.0	2.01	0.99	bzb	PKS 0010-401
2FGLJ0013.8+1907	J001356.37+191041.9	0.056	0.0034	6.0E-4	1.75	0.98	bzb	GB6 J0013+1910

Col. (1) 2FGL name.
Col. (2) *WISE* name of the WBC candidate counterpart.
Col. (3) p value computed with the positional association procedure (see Section 3.1).
Col. (4) p value computed with the positional association procedure including the IR-γ-ray constraints (see Section 3.1).
Col. (5) $log\, LR_{ik}$ value computed with the LR method (see Section 3.2).
Col. (6) ρ value computed with the LR method (see Section 3.2).
Col. (7) Class reported in the 2FGL/2LAC for sources associated with different methods: agu= AGN of uncertain type, bzb = BL Lac object, bzq = flat spectrum radio quasars, sey = Seyfert galaxy reg = radio galaxy. Capital letters have been used to indicate identified sources.
Col. (8) Counterpart name reported in the 2FGL/2LAC for sources associated with different methods.

TABLE 2
Association probabilities for 1FGL sources.

1FGL name	WBC association	R deg.	p pos.	p IR cons.	$log\, LR_{ik}$	ρ	1FGL class	1FGL counterpart
1FGLJ0041.9+2318	J004204.55+232001.1	0.043	0.0016	2.0E-4	1.46	0.96	bzq	PKS 0039+230
1FGLJ0147.4+1547	J014716.88+154943.9	0.05	0.0025	4.0E-4	1.76	0.98		
1FGLJ0305.0-0601	J030500.56-060741.5	0.108	0.0174	0.0101	1.29	0.94	bzb	CRATES J0305-0607
1FGLJ0422.1+0211	J042252.21+021926.9	0.228	0.0567	0.044	0.8	0.9	bzq	PKS 0420+022
1FGLJ0622.3-2604	J062222.06-260544.6	0.023	2.0E-4	0.0	2.18	0.99	agu	CRATES J0622-2606
1FGLJ0659.9+1303	J070014.31+130424.4	0.076	0.0079	0.0026	1.83	0.98		
1FGLJ0835.4+0936	J083543.20+093717.9	0.063	0.0047	—	1.75	0.98	bzb	CRATES J0835+0937
1FGLJ0849.4-2912	J084922.10-291150.4	0.019	1.0E-4	0.0	1.84	0.98		
1FGLJ0949.8+1757	J094939.75+175249.4	0.082	0.0095	0.0036	1.49	0.96	bzq	CRATES J0949+1752
1FGLJ1220.2+3432	J122008.29+343121.7	0.023	2.0E-4	0.0	1.67	0.98	bzb	CGRaBS J1220+3431
1FGLJ1322.1+0838	J132210.17+084232.9	0.062	0.0046	0.0010	1.6	0.97		
1FGLJ1422.7+3743	J142245.16+374915.8	0.095	0.0132	0.0064	0.96	0.89	bzb	CLASS J1423+3737
1FGLJ1422.7+3743	J142304.62+373730.6	0.119	0.0209	—	0.83	0.9	bzb	CLASS J1423+3737
1FGLJ1616.1+4637	J161603.77+463225.4	0.087	0.0107	0.0044	0.66	0.85	bzq	CRATES J1616+4632
1FGLJ1616.1+4637	J161614.81+464938.7	0.202	0.0484	0.0377	0.44	0.93	bzq	CRATES J1616+4632
1FGLJ1735.4-1118	J173527.18-111734.2	0.022	2.0E-4	0.0	2.55	1.0	agu	CRATES J1735-1117
1FGLJ1804.1+0336	J180356.26+034107.3	0.097	0.0137	0.0068	1.73	0.98	bzq	CRATES J1803+0341
1FGLJ2008.6-0419	J200824.43-041829.1	0.059	0.0039	8.0E-4	1.47	0.96	agn	3C 407
1FGLJ2117.8+0016	J211817.39+001316.9	0.115	0.0196	—	1.49	0.96	bzq	CRATES J2118+0013
1FGLJ2133.4+2532	J213314.36+252859.0	0.08	0.0089	0.0032	1.81	0.98		

Col. (1) 1FGL name.
Col. (2) *WISE* name of the WBC candidate counterpart.
Col. (3) p value computed with the positional association procedure (see Section 3.1).
Col. (4) p value computed with the positional association procedure including the IR-γ-ray constraints (see Section 3.1).
Col. (5) $log\, LR_{ik}$ value computed with the LR method (see Section 3.2).
Col. (6) ρ value computed with the LR method (see Section 3.2).
Col. (7) Class reported in the 1FGL/1LAC for sources associated with different methods: agu= AGN of uncertain type, bzb = BL Lac object, bzq = flat spectrum radio quasars, sey = Seyfert galaxy reg = radio galaxy. Capital letters have been used to indicate identified sources.
Col. (8) Counterpart name reported in the 2FGL/2LAC for sources associated with different methods.

5.2. *Second method: the likelihood ratio procedure*

In this section we briefly compare the variation of the likelihood ratio technique (see Section 3.2), and the one adopted in the 2LAC (Ackermann et al. 2011).

The main difference resides in the use of the IR color distributions of the WBC catalog extracted on the basis of the IR-γ-ray connection rather than the radio logN-logS distribution. Our likelihood procedure is also based on the local surface density of “background” objects to take into account sky distribution of the *Fermi* sources (as suggested by Sutherland & Saunders 1992).

Ackermann et al. (2011) adopted the integrated all-sky radio logN-logS distribution to calculate the number of “background” objects above a radio flux density S_i chosen for each radio potential counterpart within the positional uncertainty of a given *Fermi* source: $N(> S_i)$ (see Equation 2 of Ackermann et al. 2011). This could be improved selecting a particular range of expected radio flux densities chosen for example on the basis of the radio-γ-ray correlation (e.g., Ghirlanda et al. 2010; Mahony et al. 2010; Abdo et al. 2010b; Petrov et al. 2013; Massaro et al. 2013a). As we performed in our procedure while computing $Q(\Delta\, c_{12}, \Delta\, c_{34})$ and $N(\Delta\, c_{12}, \Delta\, c_{34})$ using their differential IR colors distributions. In addition, $N(> S_i)$ was not evaluated locally but assuming that the surface density of the radio survey was constant. These criteria adopted in the computation of $N(> S_i)$ could lead to low values of the likelihood ratios being less rigorous as stated by Sutherland & Saunders (1992).

In particular, using $N(> S_i)$ implies that, having two or more radio potential counterparts that lie at similar distance (i.e.,. similar r_{ik} and thus same $f(r_{ik})$) from the location of a γ-ray source but all within its positional uncertainty region, the brightest radio source has a larger value of $log\, LR_{ik}$ and thus a smaller probability to be a spurious associations (see Equation 2 in Section 3.2). There is no a priori reason to favor brightest objects since according to the radio logN-logS distributions are the rarest, as occurs when considering $N(> S_i)$. This ap-

TABLE 3
Roma-BZCAT sources not found by the Bayesian procedure.

2FGL name	2LAC class	2LAC counterpart	Roma-BZCAT name	R deg.
2FGLJ0024.5+0346	bzq	GB6 J0024+0349	BZQJ0024+0349	0.055
2FGLJ0037.8+1238	bzb	NVSS J003750+123818	BZBJ0037+1238	0.012
2FGLJ0043.7+3426	bzq	GB6 J0043+3426	BZQJ0043+3426	0.01
2FGLJ0047.9+2232	bzq	NVSS J004802+223525	BZQJ0048+2235	0.054
2FGLJ0105.3+3930	bzb	GB6 J0105+3928	BZUJ0105+3928	0.062
2FGLJ0115.4+0358	bzb	PMN J0115+0356	BZBJ0115+0356	0.049
2FGLJ0342.4+3859	bzq	GB6 J0342+3858	BZQJ0342+3859	0.028
2FGLJ0515.5+7355	bzb	GB6 J0516+7350	BZBJ0516+7351	0.101
2FGLJ0515.9+1528	bzb	GB6 J0515+1527	BZBJ0515+1527	0.039
2FGLJ0517.5+0900	bzq	PMN J0517+0858	BZQJ0517+0858	0.047
2FGLJ0648.9+1516	agu	VERITAS J0648+152	BZBJ0648+1516	0.027
2FGLJ0849.2+6606	bzb	GB6 J0848+6605	BZBJ0848+6606	0.036
2FGLJ0941.4+2724	bzq	MG2 J094148+2728	BZUJ0941+2722	0.108
2FGLJ1048.6+2336	bzb	NVSS J104900+233821	BZUJ1049+2328	0.091
2FGLJ1251.2+1045	bzb	1RXS J125117.4+103914	BZBJ1251+1039	0.106
2FGLJ1330.9+7001	bzb	NVSS J133025+700141	BZBJ1330+7001	0.045
2FGLJ1520.8-0349	bzb	NVSS J152048-034850	BZBJ1520-0348	0.026
2FGLJ1649.6+5238	bzb	87GB 164812.2+524023	BZBJ1649+5235	0.071
2FGLJ1754.3+3212	bzb	RX J1754.1+3212	BZBJ1754+3212	0.03
2FGLJ1810.8+1606	bzb	87GB 180835.5+160714	BZBJ1810+1608	0.039
2FGLJ1811.3+0339	bzb	NVSS J181118+034114	BZBJ1811+0341	0.032
2FGLJ1836.2+3137	bzb	RX J1836.2+3136	BZBJ1836+3136	0.015
2FGLJ1841.7+3221	bzb	RX J1841.7+3218	BZBJ1841+3218	0.042

Col. (1) 2FGL name.
Col. (2) Class reported in the 2LAC for sources associated with different methods: agu= AGN of uncertain type, bzb = BL Lac object, bzq = flat spectrum radio quasars.
Col. (3) Counterpart name reported in the 2LAC for sources associated with different methods. Col. (4) Roma-BZCAT name of the candidate counterpart.
Col. (5) Angular separation between the Roma-BZCAT and the 2FGL positions.

proach appears to be less accurate when applied to faint radio sources since their density increases as their radio flux density decreases.

Given the radio-γ-ray connection, it is thus expected that faint γ-ray sources should be associated with faint radio objects. Thus the use of the integrated radio logN-logS distribution to determine the surface density of "background" objects could lead to an "incorrect" associations if a spurious bright source lies by chance closer to a faint *Fermi* object. Our approach is less affected by the previously discussed "the brightest the most favored" problem or a similar one defined for the integrated distributions of the IR colors, that occurs when using a flux density or a magnitude integrated distribution rather than the differential one (see also Sutherland & Saunders 1992).

There is also another difference in the equations used to estimate the LR_{ik} between our method and the one described in Ackermann et al. (2011, see also Masci et al. 2001) As described by Sutherland and Saunders (1992), we are taking into account the probability $Q(\Delta c_{12}, \Delta c_{34})$ while according to the Ackermann et al. (2011) definition, this was set to 1.

Regarding the local estimates of $Q(\Delta c_{12}, \Delta c_{34})$ and $N(\Delta c_{12}, \Delta c_{34})$, it is difficult to justify and assume a constant density of the potential radio counterparts over the survey footprint, (see Section 3.2 of Ackermann et al. 2011) whenever the radio survey covers several hundreds of square degrees in the sky as the NVSS (Condon et al. 1998) or the SUMSS cases (Mauch et al. 2003). To highlight the relevance of taking into account the local source density, we show in Figure 12 the Hammer projection of the northern region of the SUMSS catalog (Mauch et al. 2003), where the differences between the source density in different regions are mild but evident. This situation is even more emphasized in the case of the *WISE* all-sky survey and on it sky distribution of the WBC catalog (D'Abrusco et al. 2014). This effect could be also a

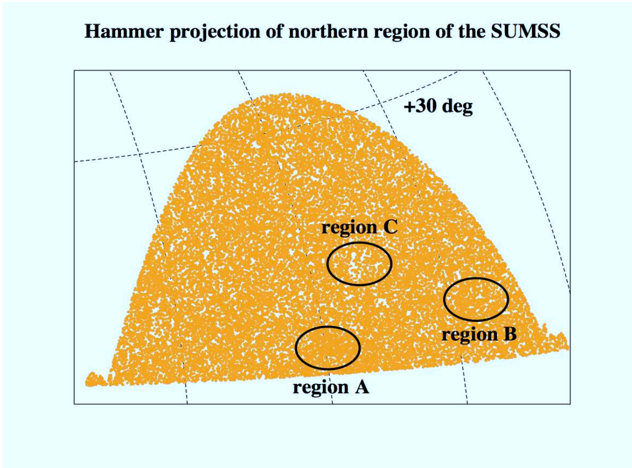

Fig. 12.— The Hammer (i.e., equal-area) projection of the source sky distribution in the northern region covered by the SUMSS (Mauch et al. 2003). It is clear how the surface density of radio sources could vary locally. For instance, the elliptical region (A) has a larger surface density with respect to region B or even more with respect to region C, whereas all the three ellipses have the same area. This stresses the idea of using the local surface density when computing $N(\Delta c_{12}, \Delta c_{34})$ in a comparison catalog.

problem when the *Fermi* source lies on the edge of the radio survey footprint where this situations does not occur in the *WISE* since it covers the entire sky. In Figure 13 we also show the total number of NVSS radio sources within a circular region of 0.2° radius computed around the γ-ray positions of the 2FGL sources at different Galactic latitudes. Despite the fact that the average NVSS source density is quite uniform above and below the Galactic plane (Condon et al. 1998), it is quite evident that the fluctuations around its mean value could be up a factor of $\sim$8 even if at high Galactic latitudes. This indicates that the assumption of considering constant such density of "background" objects could reduce the number of reliable associations when using a radio

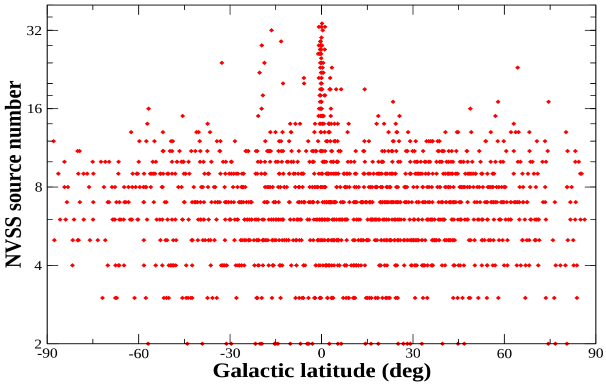

FIG. 13.— The total number of NVSS radio sources within a circular region of 0.2° radius counted around the γ-ray positions of the 2FGL sources at different Galactic latitudes. It is clear how the NVSS source density fluctuates around its mean value even at high Galactic latitudes.

survey as the NVSS searching for the low-energy counterparts of *Fermi* sources as performed in the 2LAC.

Finally, we also highlight that computing and restricting the ranges of Δc_{12} and Δc_{34} using the correlation between the γ-ray spectral index and the IR colors allows to avoid spurious associations. As previously noticed it reduces the surface density of the blazar-like candidates by ∼10-15% but for a *Fermi* sources with a spectral index α_γ very different from that of blazars (e.g., PSRs), this effect is much more relevant leading to a WBC density reduced by up 95% or even more. Form Figure 9, it is clear that for sources with $\alpha_\gamma = 0.25$, there are basically no expected WBC sources that could be a potential counterpart.

6. SUMMARY AND CONCLUSIONS

We have presented two methods to determine the association probability related to the comparison between the WBC catalog and the current available *Fermi* catalogs (i.e., 1FGL and 2FGL Abdo et al. 2010a; Nolan et al. 2012). The former procedure is based on Montecarlo simulations and it takes into account the sky distribution of the sources in the comparing catalog. The latter is a variation of the likelihood ratio method (e.g., Sutherland & Saunders 1992; Masci et al. 2001) whereas the underlying parameters used to compute the sources densities are not their magnitudes or their fluxes but their IR colors. This allows us to take into account the underlying correlation between the IR and the γ-ray spectral shape found for the *Fermi* blazars (Massaro et al. 2011a; D'Abrusco et al. 2012) and used to extract the WBC catalog (D'Abrusco et al. 2014).

Once the reliability thresholds for each method were established, we selected the associated sources in the comparison WBC catalog for the 2FGL sources and for a subsample of 1FGL sources, not listed in the 2FGL. Our associations are in agreement with previous analyses but we also found new potential counterparts of several UGSs. In particular, 39 UGSs of the 2FGL and 5 of those listed in the 1FGL have now at least one potential counterpart, being a γ-ray blazar-like source, to which an association probability has been assigned as required for the sources listed in the *Fermi* catalogs. It is also worth noting that none of PSRs listed in the second pulsar LAT catalog (Abdo et al. 2013) has a γ-ray blazar-like source located within their *Fermi* positional uncertainty region This is in agreement with the fact that the chance of spurious associations for our WBC potential counterparts is extremely low all over the sky.

We highlight that all the UGSs associated with a WBC counterpart in the 2FGL or in the 1FGL analyses presented here were not listed in any of the previous *Fermi* catalogs, and now thanks to their assigned association probability they could be included in future releases. It is also worth mention that our association procedures indicates as reliable correspondences many AGUs that having also peculiar IR colors have a larger chance to be blazar-like sources. Then it is also relevant to point that both procedures lists among their reliable associations several Seyfert galaxies included in the 2FGL and classified as radio-loud narrow-line Seyfert 1 (RLNLSy1; e.g., Komossa et al. 2006; Abdo et al. 2009). This strongly supports the underlying connection between the γ-ray emission and the peculiar IR colors used to extract our WBC catalog and could indicate that these RLNLSy1 are more similar to blazars than expected (e.g., Foschini et al. 2011; D'Ammando et al. 2012; D'Ammando et al. 2013).

Finally, we emphasize that extensive ground-based spectroscopic observations in the IR-optical are necessary to verify the nature of the selected *WISE* counterparts and to estimate the fraction of non-blazar objects eventually present in the WBC catalog, as already performed for the *Fermi* UGSs (Masetti et al. 2013a; Paggi et al. 2014) similarly to the INTEGRAL follow up campaigns (e.g., Masetti et al. 2010; Masetti et al. 2012; Masetti et al. 2013b).

F. Massaro is grateful to the colleagues of the Fermi LAT collaboration, in particular to S. Digel J. Ballet, and B. Lott for their valuable comments. The work is supported by the NASA grants NNX12AO97G and NNX13AP20G. Part of this work is based on archival data, software or on-line services provided by the ASI Science Data Center. This research has made use of data obtained from the high-energy Astrophysics Science Archive Research Center (HEASARC) provided by NASA's Goddard Space Flight Center; the SIMBAD database operated at CDS, Strasbourg, France; the NASA/IPAC Extragalactic Database (NED) operated by the Jet Propulsion Laboratory, California Institute of Technology, under contract with the National Aeronautics and Space Administration. Part of this work is based on the NVSS (NRAO VLA Sky Survey): The National Radio Astronomy Observatory is operated by Associated Universities, Inc., under contract with the National Science Foundation. This publication makes use of data products from the Wide-field Infrared Survey Explorer, which is a joint project of the University of California, Los Angeles, and the Jet Propulsion Laboratory/California Institute of Technology, funded by the National Aeronautics and Space Administration. TOP-

CAT[7] (Taylor 2005) for the preparation and manipulation of the tabular data and the images.

REFERENCES

Abdo, A. A., et al. 2009, ApJ, 707, L142
Abdo, A. A. et al. 2010a ApJS 188 405
Abdo, A. A. et al. 2010b ApJ, 715, 429
Abdo, A. A. et al. 2013 ApJS, 208, 17
Ackermann, M. et al. 2011 ApJ, 743, 171
Atwood, W. B. et al. 2009 ApJ, 697, 1071
Baumgartner, W. H. et al. 2013 ApJS, 207, 19
Barthelmy, S.D. et al., 2005 SSR, 120, 143
Becker, R. H., et al. 1995 ApJ, 450, 559
Blandford, R.D. & Rees, M.J., 1978, in Proc. Pittsburgh Conf. on BL Lac objects, (Pittsburgh, PA: Univ. Pittsburgh), 328
Condon, J. J. et al. 1998, AJ, 115, 1693
Cowperthwaite, Philip S. et al. 2013 AJ, 146, 110
Cutri et al. 2012 wise.rept, 1C
D'Abrusco, R. et al. 2012 ApJ, 748, 68
D'Abrusco, R. et al. 2013 ApJS, 206, 12
D'Abrusco , R. et al. 2014 ApJS submitted
D'Ammando, F. et al. 2012 MNRAS, 426, 317
D'Ammando, F. et al. 2013 MNRAS, 436, 191
de Ruiter, H. R., Willis, A. G., Arp, H. C. 1977 A&AS, 28, 211
Foschini, L., et al. 2011, MNRAS, 413, 1671
Gehrels, N. et al., 2004, ApJ, 611, 1005
Ghirlanda, G. et al. 2010 MNRAS, 407, 791
Komossa, S. et al. 2006, AJ, 132, 531
Laurent-Muehleisen, S.A. et al., 1999, ApJ, 525, 127
Lonsdale, C. et al. 1998, in IAU Symp. 179, New Horizons from Multi-Wavelength Sky Surveys, ed. B. J. McLean, D. A. Golombek, J. J. E. Hayes, & H. E. Payne (Cambridge: Cambridge Univ. Press), 450
Mahony, E. K. et al. 2010 ApJ, 718, 587
Masci, F. J. et al. 2001, PASP, 113, 10
Masetti, N. et al. 2010 A&A, 519A, 96
Masetti, N. et al. 2012 A&A, 538A, 123
Masetti, N. et al. 2013a A&A, 559, 58
Masetti, N. et al. 2013b A&A, 556, 120
Massaro, E. et al. 2009 A&A, 495, 691
Massaro, F. et al. 2011a ApJ, 740L, 48
Massaro, E. et al. 2011b "Multifrequency Catalogue of Blazars (3rd Edition)", ARACNE Editrice, Rome, Italy
Massaro, F. et al. 2012b ApJ, 752, 61
Massaro, F., 2012b ApJ, 750, 138
Massaro, F. et al. 2013a ApJS, 207, 4
Massaro, F. et al. 2013b ApJS, 209, 10
Massaro, F. et al. 2013c ApJS, 206, 13
Massaro, F. et al. 2014 ApJS in prep.
Mattox, J. R., Schachter, J., Molnar, L., Hartman, R. C., Patnaik, A. R. 1997 ApJ, 481, 95
Mauch, T. et al. 2003 MNRAS, 342, 1117
Nolan et al. 2012 ApJS, 199, 31
Paggi, A. et al. 2013 ApJS, 209, 9
Paggi, A. et al. 2014 AJ accepted
Petrov, L. et al. 2013 MNRAS, 432, 1294
Prestage, R. M., & Peacock, J. A., 1983, MNRAS, 204, 355
Richter, G. A., 1975, Astroh. Nachrichten, 296, 65
Stickel, M. et al. 1991 ApJ, 374, 431
Stocke et al. 1991, ApJS, 76, 813
Sutherland, W. & Saunders, W. 1992 MNRAS, 259, 413
Taylor, M. B. 2005, ASP Conf. Ser., 347, 29
Urry, C. M., & Padovani, P. 1995, PASP, 107, 803
White, R. L. et al. 1997 ApJ, 475, 479
Wolstencroft, R. D. et al. 1986, MNRAS, 223, 279
Wright, E. L., et al. 2010 AJ, 140, 1868

[7] http://www.star.bris.ac.uk/~mbt/topcat/